Geochemistry Geophysics Geosystems G3

Published by AGU and the Geochemical Society

Article
Volume 13, Number 1
7 December 2012
Q0AM05, doi:10.1029/2012GC004301
ISSN: 1525-2027

Detailed volcanostratigraphy of an accreted seamount: Implications for intraplate seamount formation

Susan R. Schnur
College of Earth, Ocean, and Atmospheric Sciences, Oregon State University, 104 CEOAS Administration Building, Corvallis, Oregon 97331, USA (sschnur@coas.oregonstate.edu)

Lisa A. Gilbert
Maritime Studies Program of Williams College and Mystic Seaport, 75 Greenmanville Avenue, Mystic, Connecticut 06355, USA (lgilbert@williams.edu)

[1] Seamounts are a ubiquitous feature of the seafloor but relatively little is known about their internal structure. A seamount preserved in the Franciscan mélange of California suggests a sequence of formation common to all seamounts. Field mapping, geophysical measurements, and geochemical analyses are combined to interpret three stages of seamount growth consistent with the formation of other intraplate seamounts such as the Hawaiian volcanoes and the island of La Palma. A seamount begins to form as a pile of closely packed pillows with a high density and low porosity. Small pillow mound volcanoes common at mid-ocean ridges are seamounts that do not grow beyond this initial stage of formation. The second stage of seamount formation is marked by the first occurrence of breccia. As the seamount grows and becomes topographically more complex, slope varies and fractured material may begin to accumulate. Magma supply may also become spatially diffuse as the seamount grows and new supply pathways develop through the edifice. The second stage thus exhibits variability in both flow morphologies and geophysical properties. The final cap stage is composed of thin flows of various morphologies. These sequences reflect the shoaling of the seamount and a greater variability in extrusion rate resulting from waning magma supply and increased mass wasting. Understanding the growth and structure of seamounts has important implications for intraplate volcanism and for models of hydrothermal circulation in the oceanic crust.

Components: 6000 words, 7 figures.

Keywords: ophiolites; pillow lavas; porosity; seamounts.

Index Terms: 3037 Marine Geology and Geophysics: Oceanic hotspots and intraplate volcanism; 3042 Marine Geology and Geophysics: Ophiolites (8140); 3075 Marine Geology and Geophysics: Submarine tectonics and volcanism.

Received 18 June 2012; **Revised** 25 October 2012; **Accepted** 27 October 2012; **Published** 7 December 2012.

Schnur, S. R., and L. A. Gilbert (2012), Detailed volcanostratigraphy of an accreted seamount: Implications for intraplate seamount formation, *Geochem. Geophys. Geosyst.*, *13*, Q0AM05, doi:10.1029/2012GC004301.

Theme: Studies of Seamount Trails: Implications for Geodynamic Mantle Flow Models and the Geochemical Evolution of Primary Hot Spots

1. Introduction

[2] The distribution of flow morphologies within a seamount is a detailed record of variations in magma supply rate over time, providing insight into the processes driving intraplate melt generation [*Staudigel and Clague*, 2010]. Volcanostratigraphy also affects the porosity and permeability structure of seamount edifices. Since seamounts are important as potential upflow zones for hydrothermal circulation [*Fisher et al.*, 2003], understanding internal structure has implications for pathways of hydrothermal fluid and the thermal evolution of oceanic crust.

[3] The inaccessibility of seamounts has limited our understanding of how submarine volcanoes evolve throughout their eruptive histories. Previous work has examined the broad geophysical characteristics of seamount edifices via remote methods [e.g., *Hammer et al.*, 1994; *Gilbert et al.*, 2007]. Seamount surface morphology has been studied extensively via seafloor mapping and submersible observations [e.g., *Lonsdale and Batiza*, 1980; *Batiza et al.*, 1984; *Wright and Gamble*, 1999; *Clague et al.*, 2000; *Mitchell*, 2001], but these studies provide only a limited view of internal structure. More detailed records of seamount volcanostratigraphy have been made in one dimension through drilling (Hawaii Scientific Drilling Program [*Garcia et al.*, 2007]; ODP Leg 197 [*Tarduno et al.*, 2002]). Field studies of obducted fragments of seamounts have also provided detailed views of seamount internal structure [e.g., *Staudigel and Schmincke*, 1984; *Meyer*, 1996; *Corcoran*, 2000; *Buchs et al.*, 2011]. Based primarily on ophiolite and drilling studies, seamounts are thought to erupt in an initial deep-water stage composed predominantly of pillow lavas, and proceed to a final shallow-water stage characterized by pillows interlayered with hyaloclastite. An intermediate stage represents a transitional period, and is sometimes divided into flank and core stages to recognize the role of mass-wasting in forming seamount flanks.

[4] We observe two main gaps in seamount internal structure research to date: 1) cross-sections from ophiolites are often based on a set of outcrops scattered over a large area and thus paint a discontinuous and incomplete picture of volcanostratigraphy, and 2) most work has focused on geochemical changes in lava composition with little consideration of the morphology and physical properties of extrusive lavas, which are crucial to understanding both the porosity and permeability structure of seamount edifices as well as variations in magma supply rate. In this study we address these gaps by integrating meter-scale field mapping with physical properties measurements and geochemical results from an approximately 1 km continuous section of an accreted intraplate seamount.

2. Geologic Setting

[5] The Nicasio Reservoir Terrane (NRT) is an accreted complex of oceanic origin preserved in the mélange of the Franciscan Formation of western California. It is thought to have formed during the early Cretaceous, about 131–138 Ma [*Gromme*, 1984]. The terrane is limited in extent, cropping out in a narrow, approximately 30 km-long band running parallel to the coast (Figure 1a). In some locations it is overlain by sandstones and cherts, with rare occurrences of underlying gabbro [*Wright*, 1984; *Blake et al.*, 2000; *Ghatak et al.*, 2012]. Based on early studies that included mapping [*Gluskoter*, 1962; *Wright*, 1984], geochemistry and petrology [*Wright*, 1984], chert dating [*Murchey and Jones*, 1984], and petrography and geochemistry of overlying graywackes [*Wright*, 1984], *Blake et al.* [2000] called the NRT "a fragment of a Late Jurassic-Early Cretaceous ocean island (similar to Hawaii)."

[6] Paleomagnetic analysis has shown that the terrane was moved north from its original position at 18°N during the Cretaceous [*Gromme*, 1984]. The NRT remagnetized at roughly the same time as the Marin Headlands Terrane (MHT) [*Hagstrum*, 1990]. However, the MHT is significantly older, and originally formed at a different latitude than the NRT [*Curry et al.*, 1984]. Recently, a timeline of crustal generation and emplacement has been established for the Franciscan Complex and Coast Range, consistent with the NRT being formed off-axis [*Wakabayashi et al.*, 2010]. This is supported by ocean island basalt (OIB)-characteristic rare earth element patterns found for a single sample of a pillow from the NRT [*Ghatak et al.*, 2012]. Accretion timing of the NRT from ages of high-grade metamorphism (100 Ma) is similar to the mid-ocean ridge basalt (MORB) of the MHT (95 Ma) [*Wakabayashi*, 1992], but the NRT (140 Ma minimum age) has a significantly younger minimum age than the Marin Headlands (190 Ma) [*Murchey and Jones*, 1984]. Together these results suggest that the NRT is a seamount erupted onto relatively old oceanic crust, perhaps ~50 Ma.

3. Methods

[7] In the northernmost section of the NRT, lavas are exposed in terraced roadcuts for a horizontal

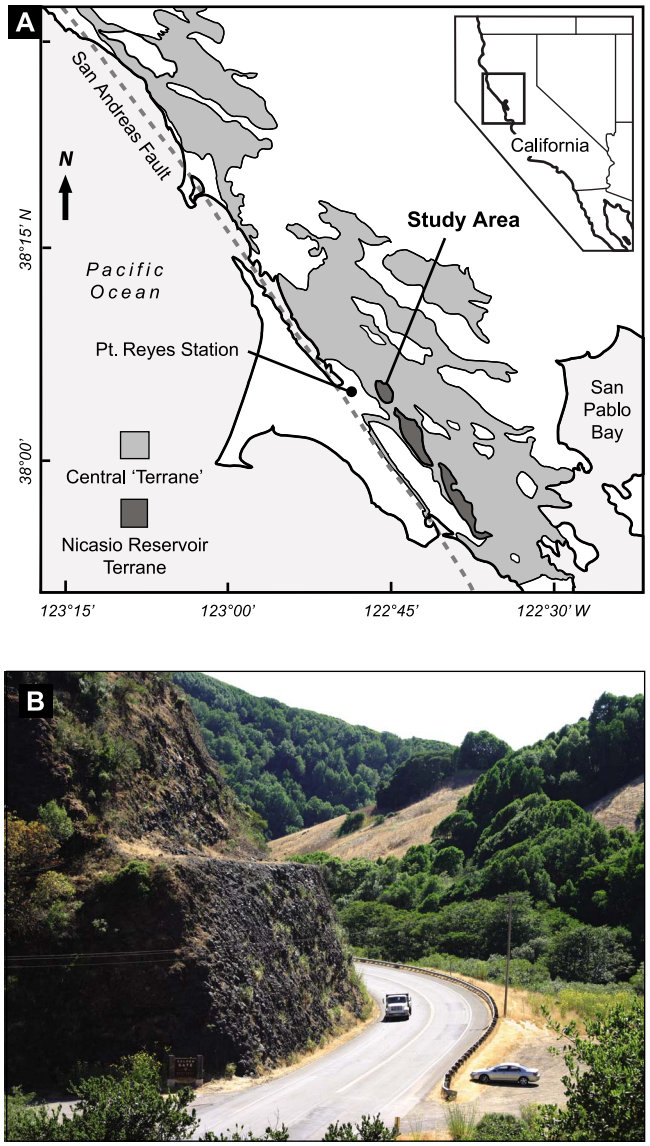

Figure 1. General study area and location of the Nicasio Reservoir Terrane (NRT) within the Central Terrane of the Franciscan Formation. Unmarked areas on land indicate Cenozoic sedimentary cover that limits access to the Mesozoic understory. The specific study area is located about 10 km east of the town of Pt. Reyes Station, California (adapted from *Blake et al.* [1984]). The photograph shows how pillows crop out in road cuts at the field area. Mapping was done by marking contacts along the road and correcting them for dip angle.

distance of about 1 km, comprising the field area for this study (Figure 1b). The lavas dip 40–60° to the NE throughout the exposures and are relatively undeformed beyond several narrow faults. Because of poor exposure for much of the NRT, the specific section studied here has yet to be placed within the larger seamount edifice.

3.1. Field

[8] The field area consists of dipping units exposed in cross-section along a roadcut. The road cuts upwards through a hillside, providing access to successive units. Unit horizontal thickness was marked at contacts along the road and then converted into vertical thickness using dip angle. Pillow lava size was measured at every site within the field area based on the methods of *Walker* [1992]. Where pillows are exposed, measurement locations were selected at 10 m intervals. At each measuring location, a 3 m line transect was marked on the vertical rock face, 1 m above the ground. The extent of each pillow intersecting the transect was marked at the outer edge of the pillow chill margin.

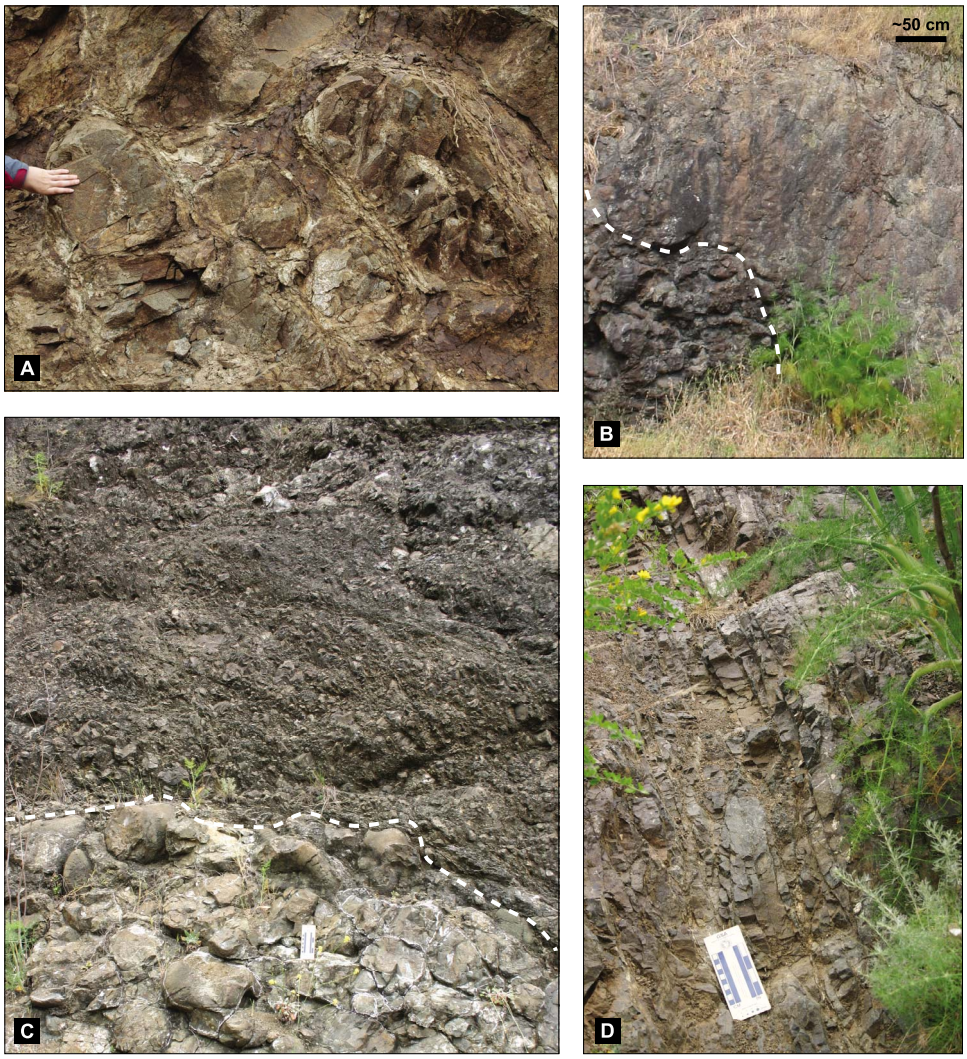

Figure 2. Five distinct facies were identified at the study area. (a) Type II pillow lavas. (b) Massive flows (top) often transition into Type I pillow lavas (bottom). (c) Type I pillow lavas (bottom). The hyaloclastite and pillow-fragment breccia facies (top) is characterized by pillow fragments and small pillow fingers embedded in a matrix of spalled glass. The size and abundance of pillow fragments in this facies varies from site to site. (d) Sheet flows appear as thin, laterally continuous layers. The solid blue scale bar shown in Figures 2c and 2d represents 10 cm.

Horizontal (H) and vertical (V) dimensions were measured at the maximum pillow length parallel and perpendicular, respectively, to the dip of pillows at each site (50 ± 10°NE). A total of 203 pillows from 21 locations were measured in this manner. Two of these measurements were rejected as outliers due to extreme aspect ratios (0.04 and 7.38, compared to a mean of 1.3–1.8) more representative of sheet flows or intrusions than pillows.

3.2. Laboratory

[9] Hand samples were cored and cut to expose fresh surfaces. From these samples, 16 thin sections were made and 10 samples were analyzed for major and trace element geochemistry with the Thermo-ARL X-ray fluorescence spectrometer at the Washington State University GeoAnalytical Lab. A total of 35 samples were analyzed for porosity, density, and specific gravity. For physical properties measurements, samples were soaked in deionized water for 24 h, with all excess air bubbles removed using a vacuum pump, then weighed wet with a Denver Instruments M-2200 electronic balance, precise to 0.0001 g. Samples were then heated in a 105 ± 5°C convection oven for 24 h, dried in a vacuum chamber with desiccant for 24 h, and weighed dry. Samples were then analyzed in a Quantachrome Pentapycnometer to determine

dry volume by helium displacement, precise to 0.001 cm^3.

[10] Specific gravity was measured with an Acculab Universal Specific Gravity Kit. Each sample was weighed dry, then weighed submerged in water. The dry weight divided by the difference between the dry weight and the weight in water is the specific gravity [see e.g., *Moore*, 2001]. Residual porosity and density were calculated using the methods of *Blum* [1997] (Method C). Specifically, grain density (ρ_g) was calculated as the dry mass (m_d) divided by the dry volume (v_d). Bulk density (ρ_b) was calculated as the wet mass divided by the sum of the dry volume and the pore water volume (v_{pw}), where pore water volume is the difference between the wet mass and the dry mass divided by the density of the pore water. Residual porosity was calculated by dividing pore water volume by the bulk volume. Original porosity was estimated from thin sections by measuring the area of all vesicles, whether filled or open, observed in 5 different 200 mm^2 fields of view for each thin section.

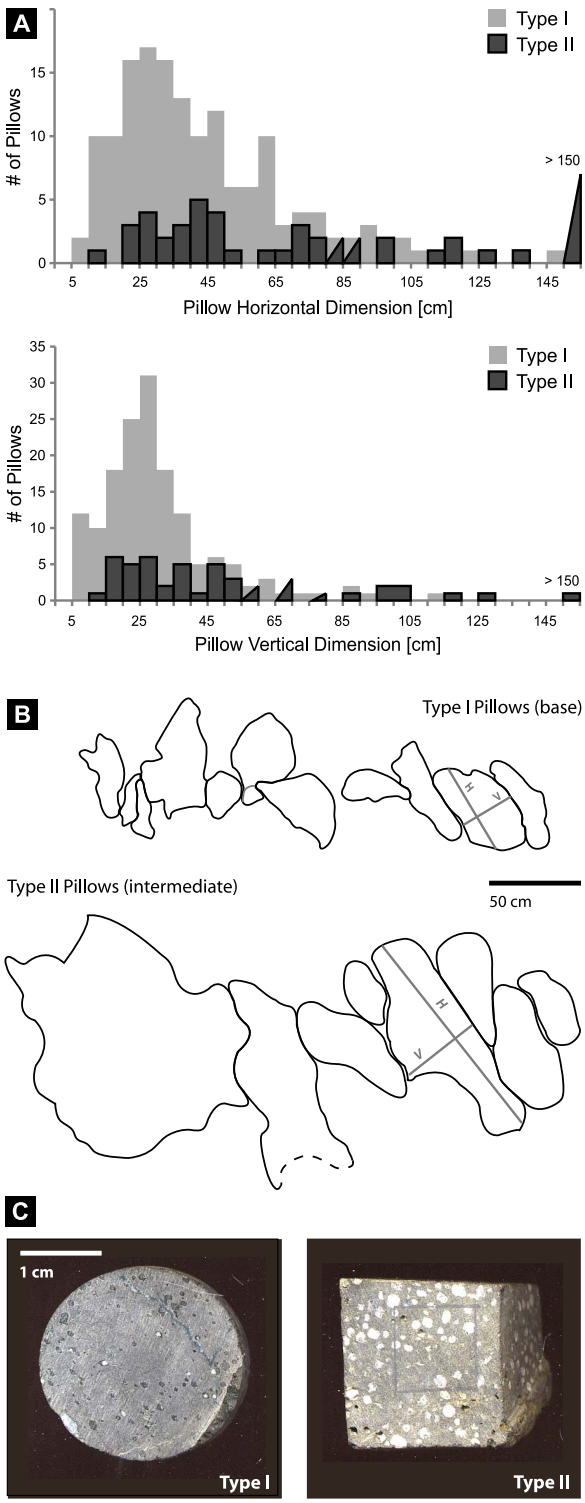

Figure 3. Distinction between Type I and Type II pillow lavas based on pillow size, morphology and vesicularity. (a) Pillow horizontal (top) and vertical (bottom) size measurements (bars are made triangular for bins where both series would overlap). Type II pillows tend to have a distribution more skewed toward the large size end of the spectrum whereas Type I pillows tend to have a more normal size distribution. (b) Pillow outlines show that Type I pillows tend to be smaller and more tightly packed than Type II pillows. (c) Differences in size, abundance, and infilling of vesicles: left: base of the basal stage; right: upper cap stage.

4. Results

4.1. Flow Morphologies

[11] Four major facies were identified in the exposed section: pillow lavas are the dominant morphology (74%) (Figures 2a and 2c), followed by massive flows (11%) (Figure 2b), hyaloclastite and pillow fragment breccias (10%) (Figure 2c) and sheet flows (2%) (Figure 2d); shear zones comprise 3% of the vertical section. The pillow lavas were further divided into two types based on thickness of inter-pillow hyaloclastite (IPH) zones. Type I pillows are small (median H = 39 with an interquartile range (IQR) of 26–50 cm; median V = 27 cm, IQR = 20–36 cm), closely packed (IPH <2 cm), and relatively fresh (Figure 3). In contrast, Type II pillows are slightly larger (median H = 64 cm, IQR = 38–104 cm; median V = 40 cm, IQR = 26–62 cm), loosely packed (IPH >2 cm), highly fractured and altered to prehnite-pumpellyite facies. Massive flows grade upward into pillow lavas at several locations. Sheet flows are relatively thin, with individual sheets measuring 5 cm in thickness. Breccias

are rich in vesicular pillow fragments and in some locations glass shards are aligned in a common flow direction.

4.2. Volcanostratigraphy

[12] The bottom 220 m of the section is composed predominantly of Type I pillow lavas (Figure 4). Facies variability increases above the first appearance of hyaloclastite breccias, with correspondingly thinner units. Between about 200 m and 600 m, units average 21 m in thickness. This part of the section is dominated by a second thick (135 m) unit of Type II pillow lavas. The second major unit of pillows is more fractured and stained a distinctive orange-yellow color, properties that may be indicative of hydrothermal alteration. The top of the section is composed of a varying sequence of thinner layers, averaging 10 m in thickness. Only pillow lava units have thicknesses greater than 40 m and most non-pillow units have thicknesses of less than 20 m.

4.3. Physical Properties

[13] Both density and specific gravity decrease slightly with height in the section and residual and original porosity increase slightly with height in the section (Figure 5). Type I pillows, which dominate in the lower portion of the section have an average bulk density of 2.85 $\pm$ 0.09 g/cm^3, residual porosity of 2.9 $\pm$ 0.9% and original porosity ranging from 4 to 15%. Type II pillows, which dominate in the upper portion of the section have a lower average bulk density of 2.67 $\pm$ 0.11 g/cm^3, with 7.4 $\pm$ 3.0% residual porosity and 17–19% original porosity.

4.4. Geochemistry

[14] NRT basalts are altered, with loss on ignition values of our samples ranging from 3.2 to 13.6 wt% (see Tables S1 and S2 in the auxiliary material).[1] We thus consider only elements immobile under conditions of low-grade metamorphism, but with high enough concentrations for accurate XRF analysis, such as Ti, Zr, Y, and Nb [*Winchester and Floyd*, 1977; *Pearce and Norry*, 1979]. Three samples plot into the alkali basalt field of the Nb/Y-Zr/TiO_2 diagram of *Winchester and Floyd* [1977] all of which are from the upper half of the section and come from different flow morphologies (sheet, massive, pillow); the rest are tholeiites (Figure 6a). The Zr/Y-Zr diagram of *Pearce and Norry* [1979] places the majority of samples in the field of within-plate basalts (Figure 6b) and the high field strength element abundances (Nb/Y–Zr/Y values) of our samples plot on the enriched side of the line separating products of enriched and depleted sources, between OIB and enriched mid-ocean ridge basalt (EMORB) (Figure 6c).

[1]Auxiliary materials are available in the HTML. doi:10.1029/2012GC004301.

5. Discussion

[15] It is difficult to determine whether the NRT represents a complete seamount section, but it seems likely that the mapped section includes parts of both the upper and lower edifice. It also seems likely that the NRT section has not been significantly rearranged during obduction, based on the consistent dip, lack of large-scale faulting and fracturing, and the preservation of fine-scale features such as spreading and stretching lines on the ends and sides of pillow lobes. The observed changes in physical properties with depth may indicate a shoaling of the seamount, and concentric rows of vesicles in pillows in the upper intermediate stage may indicate a shallow depth of formation for the upper part of the edifice [*Jones*, 1969]. Alternately, a high primary gas content may have contributed to the increase in porosity [*Harper*, 1984]. The notable lack of dikes observed at the study area may simply indicate that the preserved section did not intersect the seamount's main magma conduit. However, the great variability in layer thickness, pillow lava properties, and flow morphology distribution suggests that the section does cover a significant undisturbed vertical distance.

5.1. Lava Extrusion

[16] In most studies of seamount internal structure, pillow lavas appear to be approximately 50–75% of the volcanic edifice [*Staudigel and Schmincke*, 1984; *Meyer*, 1996; *Tarduno et al.*, 2002]. This observation is also supported by submersible flank studies of intraplate seamounts. Sampling and mapping on the west flank of Mauna Loa reveals a predominance of striated, bulbous and elongate pillows [e.g., *Wanless et al.*, 2006] and photography and dredge sampling on Lo'ihi seamount show an abundance of fresh pillow lavas with no clear stratigraphic breaks except for minimal capping sheet flows and volcaniclastic deposits [*Garcia et al.*, 2006]. These results contrast with lava morphology mapping at fast spreading mid-ocean ridges (MORs) such as the East Pacific Rise, where lobate

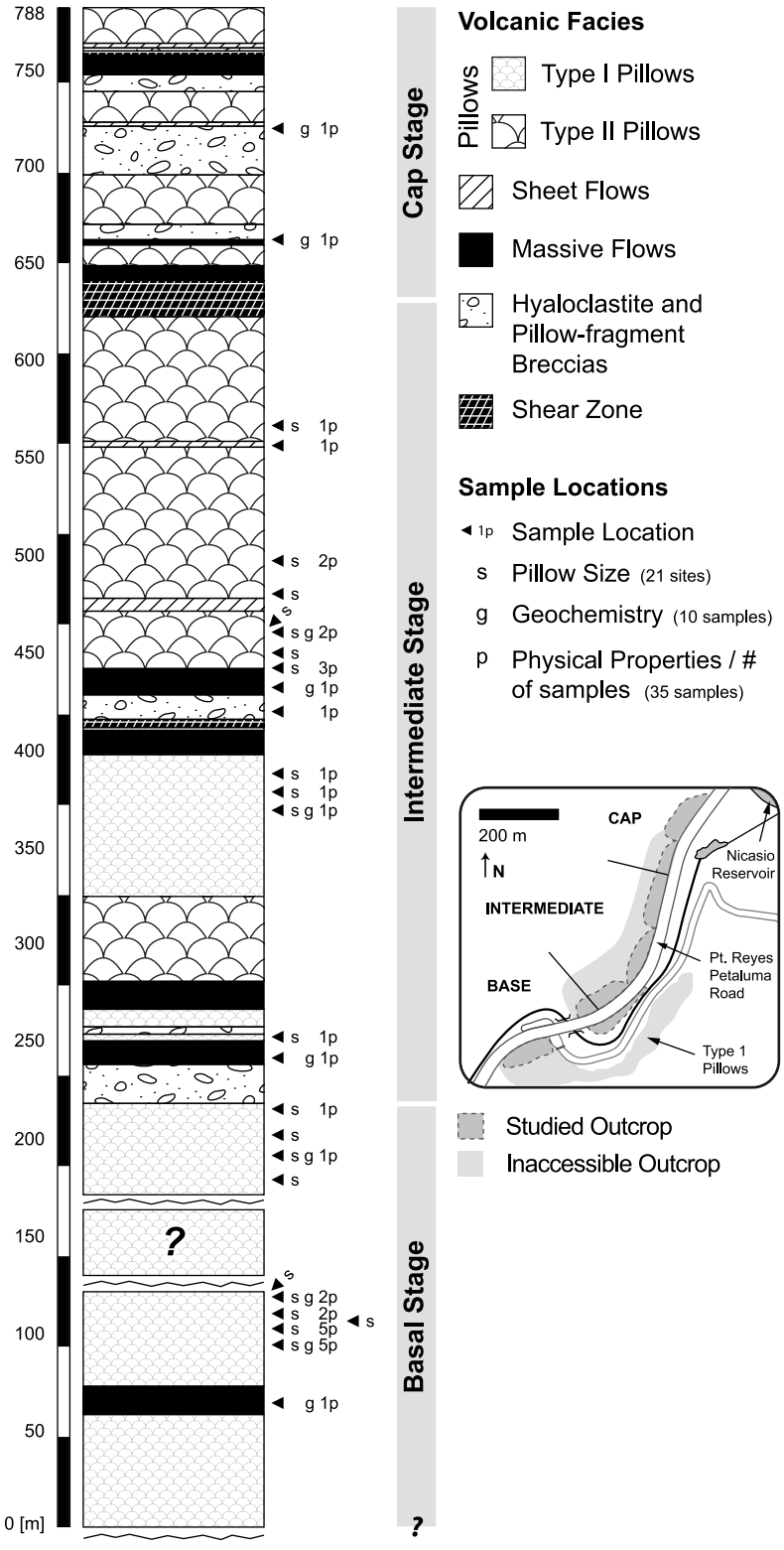

Figure 4. Outcrop stratigraphy of the NRT study area, shown to scale. Thicknesses were measured based on contacts along ~1 km of road and then corrected for dip to create a stratigraphic section. Distinctive features include a transition from Type I pillows at the bottom to Type II pillows at the top, a progressive decrease in average flow thickness with height in the section, and the presence of two major periods of pillow emplacement. Pillow size measurement and sample locations are marked to the right of the column.

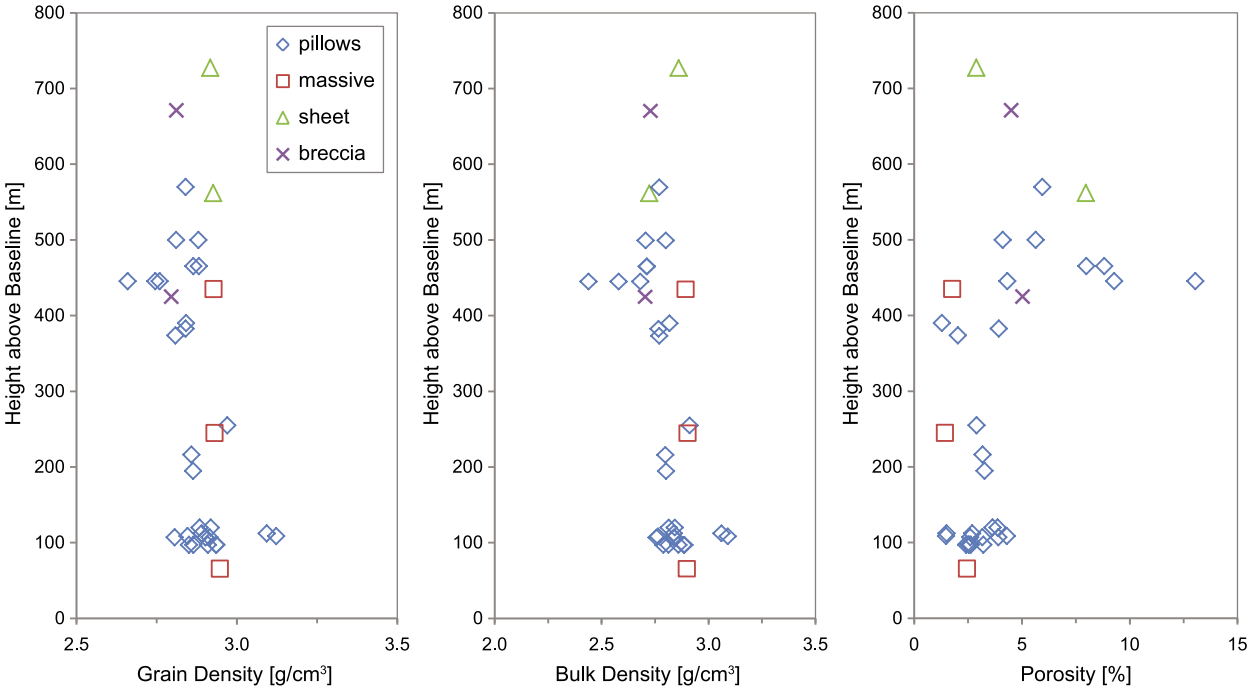

Figure 5. Variations in physical properties with height in section. Both grain density and bulk density tend to decrease with height in section and are matched by an increase in porosity.

and sheet flows tend to dominate over pillows [*Sinton et al.*, 2002; *Fundis et al.*, 2010].

[17] The lack of significant flows other than pillow lavas seems to indicate that the extrusion of other morphologies cannot be sustained for a significant period of time under seafloor conditions throughout seamount formation. The similarity observed between studies at different locations indicates a strong similarity in effusion rate at all seamounts, regardless of tectonic setting. Pillow lavas represent relatively low extrusion rates relative to cooling, whereas lobate, sheet and massive flows represent relatively high extrusion rates, assuming that lava viscosity remains constant [*Gregg and Fink*, 1995]. The predominance of pillow lavas in seamounts indicates that effusion rates are relatively low compared to dominant conditions at oceanic spreading centers. This may be due to a similarity in magma storage and supply systems for seamounts.

[18] The size and morphology of pillow lavas and the thickness of inter-pillow hyaloclastite (IPH) zones provide indicators of ambient conditions at the time of emplacement. The small, densely packed, fresh Type I pillows are indicative of emplacement at greater depths and lower extrusion rates than Type II pillows. Extrusion patterns on the ends of Type I pillow lobes show evidence of low extrusion rates (e.g., triple stretching centers), whereas Type II pillow sides show circular grooves reflecting tooth-paste-like extrusion indicative of intermediate to high extrusion rates [*Walker*, 1992]. The low volume of IPH in Type I pillows may indicate a depth control on explosive volcanism. The high volume of IPH and relatively high porosity (Figure 3) in Type II pillows may have led to increased susceptibility to infiltration by diffuse hydrothermal flow. The fractured and altered nature of the Type II pillows, with volcanic glass replaced and vesicles and fractures filled with zeolites and carbonate is characteristic of seafloor weathering seen in other ophiolites such as Troodos [e.g., *Cann and Gillis*, 2004].

5.2. Seamount Growth

[19] The NRT seamount has three distinct stages of formation, which we interpret as two major periods of pillow lava emplacement, followed by a period of waning eruptive activity (Figure 7).

5.2.1. Basal Stage

[20] The basal stage (220 m thick) resembles the structure of small pillow mound volcanoes observed at MORs, which are composed almost entirely of closely packed pillows [e.g., *Smith and Cann*, 1992; *Kennish and Lutz*, 1998]. For example, a small (200 m high) pillow mound such as those found on and near slow-spreading MORs is

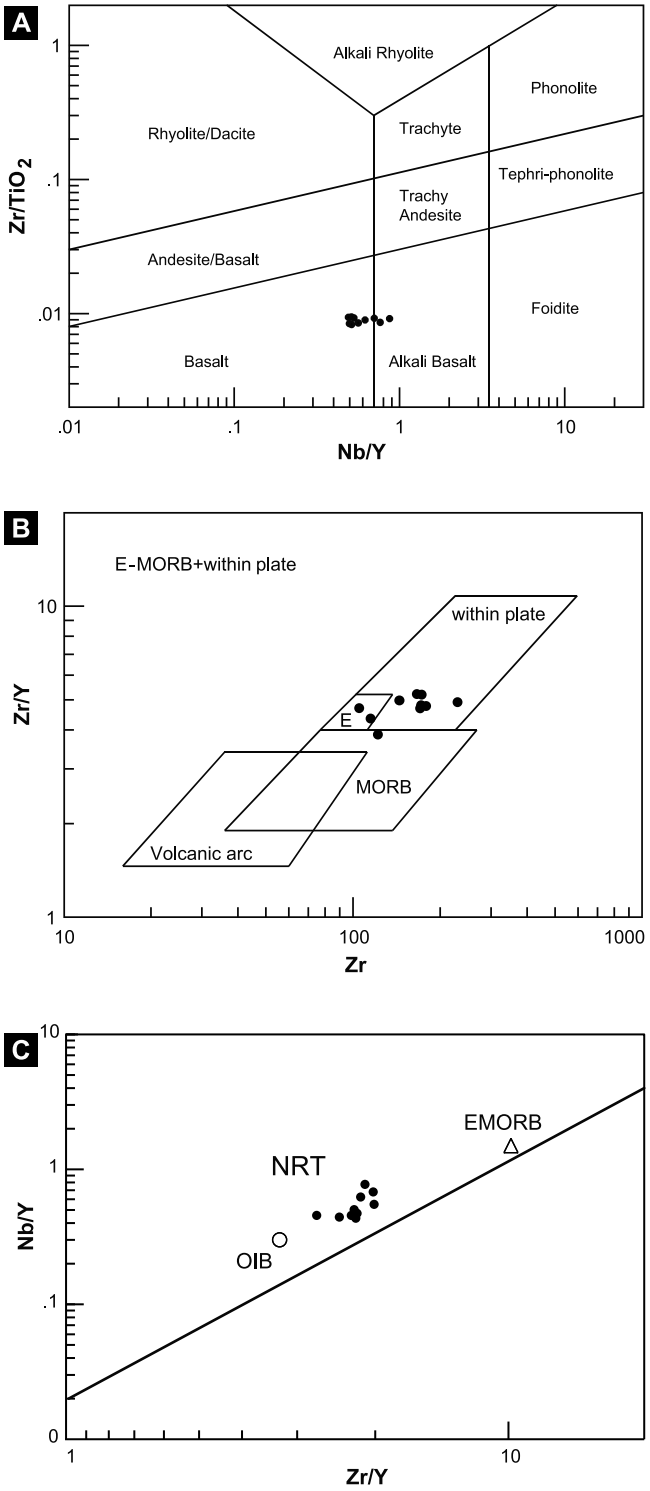

Figure 6. Geochemical variation and differentiation diagrams for elements immobile under conditions of low-grade metamorphism and low-temperature hydrothermal fluid flow. (a) Differentiation between tholeiitic and alkali basalts [*Winchester and Floyd*, 1977]. Most of the NRT rocks are tholeiitic. (b) Volcanic setting [*Pearce and Norry*, 1979]. Most points plot into the within-plate-basalt field, supporting an intraplate formation setting. (c) The NRT samples are derived from an enriched source and plot on a line between EMORB and OIB sources [after *Fitton et al.*, 1997].

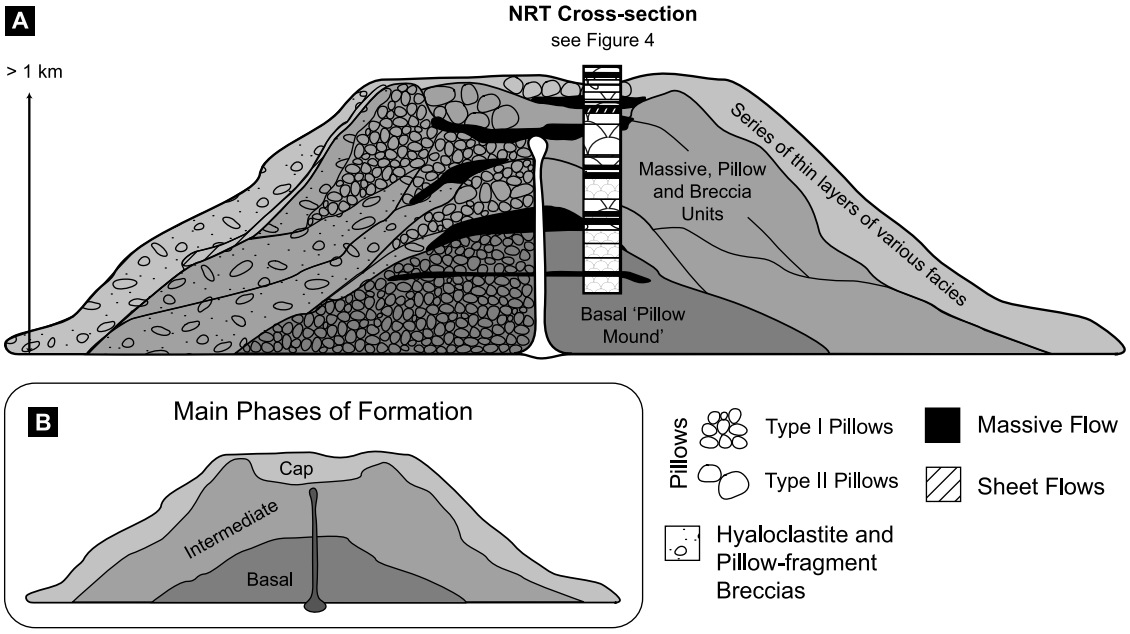

Figure 7. Generalized model of NRT seamount formation. (a) Shown here is detailed cross-section drawn based on the facies stratigraphy mapped at the study area and presented in Figure 4. A first basal stage is dominated by small, tightly packed, lower-porosity pillows which form at greater water depths atop existing oceanic crust. A second Intermediate stage is represented by a greater variety of flow types and thinner flows, occurring as a result of increasing slope. The upper portion of the intermediate stage is dominated by a second major period of pillow emplacement. Finally, a third cap stage occurs on the upper edifice of the seamount, at the end of an eruptive period. This cap stage is not dominated by a single morphology, but instead includes significant variation in flow morphology and the increased presence of sheet and HPF flows. (b) The inset shows a generalized diagram of the three stages of formation.

found in the Troodos ophiolite of Cyprus. The ophiolitic mound is composed of 80% pillows with 20% radial feeder dikes [*Eddy*, 1998]. Lo'ihi seamount, which represents a young seamount in its initial stage of growth, is dominated by pillows [*Garcia et al.*, 2006]. At Mauna Loa, a foundation of pillow lavas is covered by a thick layer of fragmental debris (>7.5 km), which is in turn covered by a thin layer of subaerial lavas [*Moore and Chadwick*, 1995]. Similarly, for the intraplate seamount La Palma, *Staudigel and Schmincke* [1984] describe an initial deep-water stage, consisting mainly of pillows. Volcaniclastic rocks begin to form only once the seamount edifice has grown larger [*Staudigel and Clague*, 2010].

5.2.2. Intermediate Stage

[21] The second, intermediate stage (middle 417 m of section) at the NRT is marked by the first occurrence of breccia, and may indicate a resurgence in magma supply following initial seamount formation. This stage introduces greater variability in flow morphologies. As the seamount grows and becomes topographically more complex, slope may vary more over short distances, and fractured material may be more common. Magma supply may also become spatially diffuse as the seamount grows and new supply pathways develop through the edifice. By comparison, at La Palma, *Staudigel and Schmincke* [1984] describe two intermediate phases: remobilized flank material and in situ deposits that were emplaced around the central conduit.

5.2.3. Cap Stage

[22] The final cap stage (top 151 m of section) at the NRT is composed entirely of thin alternating layers of different flow morphologies. These sequences reflect the shoaling of the seamount and a greater variability in extrusion rate resulting from waning magma supply. Increased mass wasting forms breccias and increased slope causes flows rather than pillows to form at low extrusion rates. Other seamounts include a final shallow-water stage characterized by pillows interlayered with hyaloclastite [e.g., *Clague and Dalrymple*, 1987; *Buchs et al.*, 2011]. At Mauna Kea, drilling revealed that the lower edifice consists predominantly of massive flows or pillow lavas, with hyaloclastite forming the

dominant facies in the upper edifice [*Stolper et al.*, 2009].

5.2.4. Geochemical Evolution

[23] The eruptive sequences observed at the NRT closely resemble those inferred from other obducted seamount fragments and the Hawaiian Islands. For example, *Buchs et al.* [2011] provide a km-scale reconstruction of an accreted intraplate volcano in Panama, interpreting three stages similar to the four broad geochemical stages in formation of Hawaiian volcanoes (alkalic pre-shield, tholeiitic shield-building, alkalic post-shield and rejuvenated) proposed by *Clague and Dalrymple* [1987]. The tholeiitic lavas of the NRT become more alkalic with height in the section, which implies a magmatic evolution similar to that of Hawaii.

5.2.5. Geophysical Models

[24] Geophysical surveys and models lend further support for the evolution of a seamount from a dense pillow core to a more complex structure capped by a less dense layer of volcaniclastic rocks. *Kellogg et al.* [1987] applied densities of 2.8 to 3.0 g/cm^3 (similar to the bulk densities of Type I pillows of this study) to the centers of seamount models to best fit gravity anomalies from two large western Pacific seamounts. On Great Meteor Seamount *Weigel and Grevemeyer* [1999] interpret distinct zones of low and high compressional wave velocity as extrusive lavas and debris flows capping a high density core located 3 km below the summit. Observations of the rifted edifice of Axial Seamount confirm the predominance of porous morphologies such as pillows and lava tubes [*Gilbert et al.*, 2007], which likely control the low bulk density and low compressional wave velocity found near the surface of seamounts like Axial [*van Heeswijk*, 1986; *Gilbert et al.*, 2007] and Jasper [*Hildebrand et al.*, 1989; *Hammer et al.*, 1994].

[25] Since pillow lavas become less abundant with height, there is increased variability in the geophysical properties of the uppermost layers of seamounts. Bulk edifice density decreases with height in the NRT. The pillow core and lower intermediate stage (0–400 m) have a combined mean bulk density of 2.85 $\pm$ 0.09 g/cm^3 and the upper intermediate stage and cap stage (400–788 m) have a combined mean bulk density of 2.72 $\pm$ 0.11 g/cm^3. Additionally, residual porosity in the bottom half of the NRT is consistently less than 4%, but varies from 2 to 13% in the upper half (Figure 5). Small seamounts which have not developed mass wasting features will thus tend to have higher overall edifice densities and lower porosities than larger, more morphologically complex seamounts.

6. Conclusions

[26] Data presented here, from an accreted seamount in California, help illuminate an important aspect of global seamount evolution. The NRT seamount shows a formation sequence exemplified by many large seamounts, consisting of: 1) An initial basal stage dominated by small, closely packed pillow lavas, 2) an intermediate stage of intermittent pillow lava emplacement and breccia formation, and 3) a final shallow-water stage that is characterized by thin layers of varying flow morphologies, indicating fluctuations in effusion rate. This process of formation is consistent with models based on data from large intraplate seamounts such as the Hawaiian Islands and La Palma. In contrast, the many small seamounts found globally likely represent only the first stage of seamount formation. Further, the density and porosity structure of the NRT seamount also reflects a pattern of seamount growth. The small, tightly packed pillows at the core of the seamount form a high-density lower layer. Higher in the edifice, breccias and larger pillows with thick altered margins result in a low-density upper layer with higher porosity and increased susceptibility to infiltration by diffuse hydrothermal flow. Since seamounts form a significant portion of the oceanic crust, these details concerning the formation and evolution of seamounts have important implications for geophysical models of oceanic crust and for heat flow and chemical budgets in the ocean.

Acknowledgments

[27] Funding was provided by Williams College, Carleton College, and a Carr Alumni Research Fellowship from the Williams-Mystic Maritime Studies Program. Comments from S. A. Soule and A.A.P. Koppers helped improve early drafts of the manuscript. Editor J. Baker and three anonymous reviewers also provided valuable feedback.

References

Batiza, R., D. J. Fornari, D. A. Vanko, and P. Lonsdale (1984), Craters, calderas, and hyaloclastites on young pacific seamounts, *J. Geophys. Res.*, *89*(B10), 8371–8390, doi:10.1029/JB089iB10p08371.

Blake, M. C., R. W. Graymer, and D. L. Jones (2000), Geologic map and map database of parts of Marin, San Francisco, Alameda, Contra Costa, and Sonoma Counties, California, *U.S. Geol. Surv. Misc. Field Stud. Map*, *MF-2337*.

Blake, M. C., D. G. Howell, and A. S. Jayko (1984), Tectonostratigraphic terranes of the San Francisco Bay Region, in *Franciscan Geology of Northern California: Pacific Section*, edited by M. C. J. Blake, *Soc. Econ. Paleontol. Mineral.*, *43*, pp. 5–22.

Blum, P. (1997), *Physical Properties Handbook: A Guide to the Shipboard Measurement of Physical Properties of Deep-Sea Cores*, Tex. A&M Univ., College Station, Tex.

Buchs, D. M., R. J. Arculus, P. O. Baumgartner, and A. Ulianov (2011), Oceanic intraplate volcanoes exposed: Example from seamounts accreted in Panama, *Geology*, *39*(4), 335–338, doi:10.1130/G31703.1.

Cann, J., and K. Gillis (2004), Hydrothermal insights from the Troodos ophiolite, Cyprus, in *Hydrogeology of the Oceanic Lithosphere*, edited by E. E. Davis and H. Elderfield, pp. 274–310, Cambridge Univ. Press, Cambridge, U. K.

Clague, D. A., and G. B. Dalrymple (1987), The Hawaiian-Emperor volcanic chain, Part 1: Geologic evolution, in *Volcanism in Hawaii*, *U.S. Geol. Surv. Prof. Pap.*, *1350*, pp. 5–54.

Clague, D. A., J. R. Reynolds, and A. S. Davis (2000), Near-ridge seamount chains in the northeastern Pacific Ocean, *J. Geophys. Res.*, *105*(B7), 16,541–16,561, doi:10.1029/2000JB900082.

Corcoran, P. L. (2000), Recognizing distinct portions of seamounts using volcanic facies analysis: Examples from the Archean Slave Province, NWT, Canada, *Precambrian Res.*, *101*, 237–261, doi:10.1016/S0301-9268(99)00090-X.

Curry, F. B., C. A. Cox, and D. C. Engebretson (1984), Paleomagnetism of Franciscan rocks of the Marin Headlands, in *Franciscan Geology of Northern California: Pacific Section*, edited by M. C. J. Blake, *Soc. Econ. Paleontol. Mineral.*, *43*, pp. 89–98.

Eddy, C. (1998), Seamount formation and associated caldera complex and hydrothermal mineralization in ancient oceanic crust, Troodos ophiolite (Cyprus), *Tectonophysics*, *292*(3–4), 189–210, doi:10.1016/S0040-1951(98)00064-X.

Fisher, A. T., et al. (2003), Hydrothermal recharge and discharge across 50 km guided by seamounts on a young ridge flank, *Nature*, *421*, 618–621, doi:10.1038/nature01316.1.

Fitton, J. G., A. D. Saunders, M. J. Norry, B. S. Hardarson, and R. N. Taylor (1997), Thermal and chemical structure of the Iceland plume, *Earth Planet. Sci. Lett.*, *153*, 197–208, doi:10.1016/S0012-821X(97)00170-2.

Fundis, A. T., S. A. Soule, D. J. Fornari, and M. R. Perfit (2010), Paving the seafloor: Volcanic emplacement processes during the 2005–2006 eruptions at the fast spreading East Pacific Rise, 9°50′N, *Geochem. Geophys. Geosyst.*, *11*, Q08024, doi:10.1029/2010GC003058.

Garcia, M. O., J. Caplan-Auerbach, E. H. De Carlo, M. D. Kurz, and N. Becker (2006), Geology, geochemistry and earthquake history of Lo'ihi Seamount, Hawaii's youngest volcano, *Chem. Erde*, *66*(2), 81–108, doi:10.1016/j.chemer.2005.09.002.

Garcia, M. O., E. H. Haskins, E. M. Stolper, and M. Baker (2007), Stratigraphy of the Hawai'i Scientific Drilling Project core (HSDP2), Anatomy of a Hawaiian shield volcano, *Geochem. Geophys. Geosyst.*, *8*, Q02G20, doi:10.1029/2006GC001379.

Ghatak, A., A. R. Basu, and J. Wakabayashi (2012), Elemental mobility in subduction metamorphism: Insight from metamorphic rocks of the Franciscan Complex and the Feather River ultramafic belt, California, *Int. Geol. Rev.*, *54*(6), 654–685, doi:10.1080/00206814.2011.567087.

Gilbert, L. A., R. E. McDuff, and H. Paul Johnson (2007), Porosity of the upper edifice of Axial Seamount, *Geology*, *35*(1), 49, doi:10.1130/G22892A.1.

Gluskoter, H. J. (1962), Geology of a portion of western Marin County, California, PhD thesis, 184 pp., Univ. of Calif., Berkeley.

Gregg, T. K. P., and J. H. Fink (1995), Quantification of submarine lava-flow morphology through analog experiments, *Geology*, *23*(1), 73, doi:10.1130/0091-7613(1995)023<0073:QOSLFM>2.3.CO;2.

Gromme, S. (1984), Paleomagnetism of Franciscan Basalt, Marin County, California, Revisited, in *Franciscan Geology of Northern California: Pacific Section*, edited by M. C. J. Blake, *Soc. Econ. Paleontol. Mineral.*, *43*, pp. 113–119.

Hagstrum, J. T. (1990), Remagnetization and northward coastwise transport of Franciscan Complex rocks, northern California: A reinterpretation of the paleomagnetic data, *Tectonics*, *9*, 1221–1233, doi:10.1029/TC009i005p01221.

Hammer, P. T. C., L. M. Dorman, J. A. Hildebrand, and B. D. Cornuelle (1994), Jasper Seamount structure: Seafloor seismic refraction tomography, *J. Geophys. Res.*, *99*(B4), 6731–6752, doi:10.1029/93JB02170.

Harper, G. D. (1984), The Josephine ophiolite, northwestern California, *Geol. Soc. Am. Bull.*, *95*(9), 1009–1026.

Hildebrand, J. A., L. M. Dorman, P. T. C. Hammer, A. E. Schreiner, and B. D. Comuelle (1989), Seismic tomography of Jasper Seamount, *Geophys. Res. Lett.*, *16*(12), 1355–1358, doi:10.1029/GL016i012p01355.

Jones, J. G. (1969), Pillow lavas as depth indicators, *Am. J. Sci.*, *267*, 181–195, doi:10.2475/ajs.267.2.181.

Kellogg, J. N., B. S. Wedgeworth, and J. T. Freymueller (1987), Isostatic compensation and conduit structures of western Pacific seamounts: Results of three-dimensional gravity modeling, in *Seamounts, Islands, and Atolls*, *Geophys. Monogr. Ser.*, vol. 43, edited by B. H. Keating et al., pp. 85–96, AGU, Washington, D. C., doi:10.1029/GM043p0085.

Kennish, M. J., and R. A. Lutz (1998), Morphology and distribution of lava flows on mid-ocean ridges: A review, *Earth Sci. Rev.*, *43*(3–4), 63–90, doi:10.1016/S0012-8252(98)00006-3.

Lonsdale, P., and R. Batiza (1980), Hyaloclastite and lava flows on young seamounts examined with a submersible, *Geol. Soc. Am Bull.*, *91*, 545–554.

Meyer, J. (1996), Off-ridge alkaline magmatism and seamount volcanoes in the Masirah island ophiolite, Oman, *Tectonophysics*, *267*(1–4), 187–208, doi:10.1016/S0040-1951(96)00094-7.

Mitchell, N. C. (2001), Transition from circular to stellate forms of submarine volcanoes, *J. Geophys. Res.*, *106*(B2), 1987–2003, doi:10.1029/2000JB900263.

Moore, J. (2001), Density of basalt core from Hilo drill hole, Hawaii, *J. Volcanol. Geotherm. Res.*, *112*(1–4), 221–230, doi:10.1016/S0377-0273(01)00242-6.

Moore, J. G., and W. W. Chadwick (1995), Offshore geology of Mauna Loa and adjacent areas, Hawaii, in *Mauna Loa Revealed: Structure, Composition, History, and Hazards*, *Geophys. Monogr. Ser.*, vol. 92, edited by J. M. Rhodes and J. P. Lockwood, pp. 21–44, AGU, Washington, D. C., doi:10.1029/GM092p0021.

Murchey, B. L., and D. L. Jones (1984), Age and significance of chert in the Franciscan Complex in the San Francisco Bay Region, in *Franciscan Geology of Northern California: Pacific Section*, edited by M. C. J. Blake, *Soc. Econ. Paleontol. Mineral.*, *43*, pp. 23–29.

Pearce, J. A., and M. J. Norry (1979), Petrogenetic implications of Ti, Zr, Y, and Nb variations in volcanic rocks, *Contrib. Mineral. Petrol.*, *69*(1), 33–47, doi:10.1007/BF00375192.

Sinton, J., E. Bergmanis, K. Rubin, R. Batiza, T. K. P. Gregg, K. C. Macdonald, and S. M. White (2002), Volcanic eruptions on mid-ocean ridges: New evidence from the superfast spreading East Pacific Rise, 17°–19°S, *J. Geophys. Res.*, *107*(B6), 2115, doi:10.1029/2000JB000090.

Smith, D. K., and J. R. Cann (1992), The role of seamount volcanism in crustal construction at the Mid-Atlantic Ridge (24°–30°N), *J. Geophys. Res.*, *97*(B2), 1645–1658, doi:10.1029/91JB02507.

Staudigel, H., and D. A. Clague (2010), The geological history of deep-sea volcanoes, *Oceanography*, *23*(1), 58–71, doi:10.5670/oceanog.2010.62.

Staudigel, H., and H. Schmincke (1984), The Pliocene seamount series of La Palm/Canary Islands, *J. Geophys. Res.*, *89*(B13), 11,195–11,215, doi:10.1029/JB089iB13p11195.

Stolper, E. M., D. J. DePaolo, and D. M. Thomas (2009), Deep drilling into a mantle plume volcano: The Hawaii Scientific Drilling Project, *Sci. Drill.*, *7*, 1–14, doi:10.2204/iodp.sd.7.02.2009.

Tarduno, J. A., R. A. Duncan, and D. W. Scholl (2002), Leg 197 summary, *Proc. Ocean Drill. Program Initial Rep*, *197*, 1–92.

van Heeswijk, M. (1986), Shallow crustal structure of the caldera of Axial Seamount, Juan de Fuca Ridge, M.S. thesis, 80 pp., Oreg. State Univ., Corvallis.

Wakabayashi, J. (1992), Nappes, tectonics of oblique plate convergence, and metamorphic evolution related to 140 million years of continuous subduction, Franciscan Complex, California, *J. Geol.*, *100*(1), 19–40, doi:10.1086/629569.

Wakabayashi, J., A. Ghatak, and A. R. Basu (2010), Suprasubduction-zone ophiolite generation, emplacement, and initiation of subduction: A perspective from geochemistry, metamorphism, geochronology, and regional geology, *Geol. Soc. Am. Bull.*, *122*(9–10), 1548–1568, doi:10.1130/B30017.1.

Walker, G. P. (1992), Morphometric study of pillow-size spectrum among pillow lavas, *Bull. Volcanol.*, *54*, 459–474, doi:10.1007/BF00301392.

Wanless, V. D., M. O. Garcia, F. A. Trusdell, J. M. Rhodes, M. D. Norman, D. Weis, D. J. Fornari, M. D. Kurz, and H. Guillou (2006), Submarine radial vents on Mauna Loa Volcano, Hawai`i, *Geochem. Geophys. Geosyst.*, *7*, Q05001, doi:10.1029/2005GC001086.

Weigel, W., and I. Grevemeyer (1999), The Great Meteor seamount: Seismic structure of a submerged intraplate volcano, *J. Geodyn.*, *28*(1), 27–40, doi:10.1016/S0264-3707(98)00030-1.

Winchester, J. A., and P. A. Floyd (1977), Geochemical discrimination of different magma series and their differentiation products using immobile elements, *Chem. Geol.*, *20*, 325–343, doi:10.1016/0009-2541(77)90057-2.

Wright, I. C., and J. A. Gamble (1999), Southern Kermadec submarine caldera arc volcanoes (SW Pacific): Caldera formation by effusive and pyroclastic eruption, *Mar. Geol.*, *161*(2–4), 207–227, doi:10.1016/S0025-3227(99)00040-7.

Wright, R. H. (1984), Geology of the Nicasio Reservoir Terrane, Marin County California, in *Franciscan Geology of Northern California: Pacific Section*, edited by M. C. J. Blake, *Soc. Econ. Paleontol. Mineral.*, *43*, pp. 99–112.